Applied Surface Science 473 (2019) 49–54

Contents lists available at ScienceDirect

Applied Surface Science

journal homepage: www.elsevier.com/locate/apsusc

Full Length Article

Electron transfer during binding processes between thiolate molecules and Au nano-islands

Bin Chen[a,*], Chuanjun Liu[b], Liang Shang[b], Ying Huang[a], Shaohua Yang[a], Xiaoyan Sun[a], Changhao Feng[a], Kenshi Hayashi[b,*]

[a] Chongqing Key Laboratory of Non-linear Circuit and Intelligent Information Processing, College of Electronic and Information Engineering, Southwest University, Chongqing 400715, China
[b] Department of Electronics, Graduate School of Information Science and Electrical Engineering, Kyushu University, Fukuoka 819-0395, Japan

ARTICLE INFO

Keywords:
Electron transfer
Localized surface plasmon resonance
Tunneling current
Au nano-islands
Thiolate molecules

ABSTRACT

We investigated electron transfer during the time-dependent binding processes between thiolate molecules and Au nano-islands by observing tunneling current with an interdigitated microelectrode supporting the sputtered Au nano-islands (IME@AuNI). The time-dependent optical and electrical signal variation during the binding process was examined for five kinds of thiolates. As the immersion time was prolonged, the optical absorbance increased, whereas the current passing through the IME@AuNI decreased. Importantly, the spectral and current characteristics depended on the thiolate structure, because of the formation of capping layer in accordance with thiolate structure. These results are mainly attributed to synergistic effects of electron transfer from Au nano-islands to thiolate molecules and bridging effects of thiolate molecules among Au nano-islands.

1. Introduction

The next generation of electroactive hybrid devices, composed of polymeric materials, nanoscopic objects, and supramolecular components requires fundamental knowledge of the dynamics of charge transport and injection at electrical contacts [1–3]. An understanding of electron transfer mechanism is needed to improve conversion efficiency in various fields, such as solar energy materials and photosensitization systems [4,5]. Investigations by Fan's group have shown that photoelectric conversion efficiency can be improved by incorporating noble metallic nanoparticles into hybrid TiO_2 photo-anodes. The use of AuNPs, AgNPs, Au nanowires (AuNWs), and AgNWs, in these experiments has indicated that incorporation of Au and Ag nanostructures leads to plasmon-enhanced sunlight absorption and increased light scattering, which increase light harvesting. The TiO_2-AgNWs sample showed strong visible-light absorption owing to plasmon-enhanced sunlight absorption, and rapid electron transfer because of the large size 1D AgNWs [5]. Reports to date have confirmed that Au nanoparticles (AuNPs) often act as effective electron accepters and donor, and as relays to facilitate electron transfer. Kamat and colleagues have reported that under steady-state and laser pulse excitation, electron transfer from TiO_2 to AuNPs depends on the diameter of the AuNPs, which influences photo-induced charge separation [6]. The use of P3HT-AuNPs as a donor layer resulted in an increased open circuit voltage and higher overall power conversion efficiency as the AuNPs content was increased. This increase was mainly attributed to additional interfaces induced by AuNPs, which facilitated charge separation of excitons and percolation pathways, which enhanced electron transfer to the TiO_2 acceptor [7]. Jensen and coworkers applied AuNPs as electron transfer relays to facilitate electronic coupling between the protein redox center cytochrome *c* and electrode surface [8].

Electron transfer is often used to explain chemical reactions and noble metallic nanoparticles composed of various materials with different structures are the most frequently selected candidates for investigating electron transfer processes. Real-time monitoring of photo-induced electron transfer (PET) process, based on chemical transformation of p-aminothiophenol (p-ATP, an important SERS signal molecule) to 4,4′-dimercaptoazobenzene on single silver nanoparticles has been examined by localized surface plasmon resonance (LSPR) spectroscopy coupled with dark-field microscopy [9]. This study visualized the PET process and provided a simple and efficient approach to explore the nature of PET and interpret the SERS mechanism in terms of p-ATP. The mechanism of the hot-hole carrier dynamics has been elucidated by studies of photo-driven oxidation of citrate ions on $Au@SiO_2@Au$ core-shell NPs. A simple theoretical model was developed to determine the probability of hot carrier-adsorbate interactions across a nanoparticle

* Corresponding authors.
E-mail address: chenbin121@swu.edu.cn (B. Chen).

https://doi.org/10.1016/j.apsusc.2018.12.138
Received 20 September 2018; Received in revised form 12 December 2018; Accepted 13 December 2018
Available online 14 December 2018
0169-4332/

surface [10]. Zhao and coworkers used facet-optimized brookite TiO_2 as a substrate and confirmed that intense visible light excitation of Au resulted in the accumulation of hot-electrons. This accumulation promoted their consecutive injections into the conduction band of TiO_2. As a result, hot-electrons with a greater reduction potential led to superior photocatalytic activity [11]. Electrochemical properties have been compared based on three different electrode fabrication techniques with different types of nanoparticle-electrode interface. The electrochemical properties of small (d_{core} < 2.5 nm) gold nanoparticles on boron doped diamond electrodes have shown electron transfer properties, which depend on the molecular tether [12].

In our previous studies, we investigated the conductance characteristics of poly (3-hexylthiophene-2,5-diyl) (P3HT)/Au nano-islands composite on interdigitated microelectrode (IME) [13,14]. The P3HT/AuNPs composite was used to fabricate an ethanol gas sensor owing to its gas concentration dependent current characteristic, which we mainly attributed to mutual interactions between AuNPs and P3HT molecules induced by ethanol molecules. These results allowed us to understand the interactions between the LSPR of the Au nano-islands and P3HT molecules. However, the role of noble metallic nanoparticles in the interfacial electron transfer is not entirely clear. Thus, in this work, we investigated the time-dependent electrical and optical characteristics during the binding process between thiolate molecules and AuNPs. The binding of thiolate molecules onto the surface of AuNPs enhanced the LSPR absorption of the AuNPs, and decreased the charge carrier mobility of Au nano-islands. Importantly, the electron transfer process was directly observed through real-time voltage-current measurements. We mainly attribute the decrease in electrical conductivity of IME@AuNI during prolonged immersion to sulfur atom limiting free electrons on AuNPs and the bridging effect of thiolate molecules between AuNPs. The results of in this study provided a new approach to observing, understanding, and applying electron transfer processes.

2. Experimental

2.1. Chemicals and materials

Thiolate agents including 2-mercaptobenzothiazole, 1-decanethiol, 1-octadecanethiol, 1-hexanethiol, 4-methoxy-α-toluenethiol, and ethanol were obtained from Tokyo Chemical Industry. All of these reagents were analytical grade, and used as received. Ultrapure deionized water produced by a Milli-Q system was used throughout this work.

2.2. IME@AuNI fabrication

The IME was prepared by photolithography [13–15], with 17 pairs of gold electrode, 25 μm width with a spacing of 33 μm (Fig. 1). The substrate was composed of a gold layer (200 nm) on Cr-primed (20 nm) glass slides. The slides were cleaned by immersion in a TL1 solution (H_2O:NH_3·H_2O:H_2O_2 = 5:1:1) and heated at 90 °C for 10 min. The slides were then rinsed with deionized water, dried in a nitrogen steam, and treated in a plasma cleaner (PDC-001, HARRICK) under an argon atmosphere. The pre-treated bare IME slides were immersed in a 1:15 (volume ratio) solution of 3-aminopropyl triethoxysilane (APTES) (Shin-Etsu Chemical) in ethanol for 1 h, rinsed in an ultrasonic bath of ethanol for 5 min, and dried at 105 °C for 10 min. Au sputtering on the APTES modified IME substrate was performed using a quick coater (SC-701HMC, Sanyu Denshi, Japan) under sputtering conditions with a sputtering current of 1.5 mA and a sputtering time of 160 s. Next, thermal annealing was performed in air at 120 °C for 10 min in a muffle furnace (ISUZU SSTS-13K, ISUZU, Japan). The annealed slides were allowed to cool to room temperature. The working area of the electrode was controlled with the use of a chemically inert adhesive polyimide tape to give an exposed area of 0.0625 cm^2.

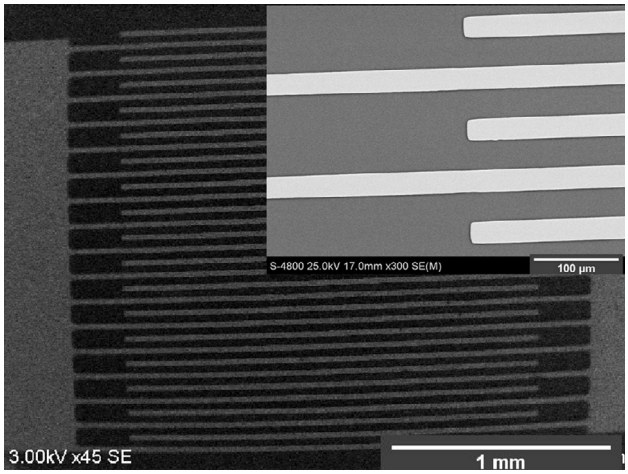

Fig. 1. SEM image of the as-prepared IME.

2.3. Equipment

A scanning electron microscope (SEM, SU8000, Hitachi, Japan) was used to characterize the morphology and distribution of the Au nano-islands deposited on IME substrates. A UV–vis spectrophotometer (UV1800, Shimadzu, Japan) was used to measure the absorbance of the Au nano-islands film. The scanning range was changed from 400 nm to 1000 nm (resolution: 1 nm).

2.4. Voltage-Current measurements

The resistance of Au nano-islands monolayer was high, which presented a challenge for the measurement setup. IME with a narrow interdigital space on the micrometer scale can effectively decrease the initial resistance. The current-voltage characteristics of the bare IME substrates were measured with the system presented in Fig. 2. The output voltage from a precision source/measure unit (SMU, B2920A, Agilent, USA) was swept linearly from 0 to 1 V (step: 20 mV). An aluminum alloy box was set on an anti-vibration table, to avoid external vibrations and electromagnetic interference. The electrical signal from the SMU was transmitted through the side of the box by a triaxial cable. In addition to the anode and cathode, an extra reference electrode was connected to the electromagnetic shielding box. The IME@AuNI substrate was inserted into 5 mL ethanol or thiolate ethanol solution in a small Petri dish, and covered by a plastic container. The voltage-current curve was measured at 3-min intervals to observe the time-dependent response characteristics.

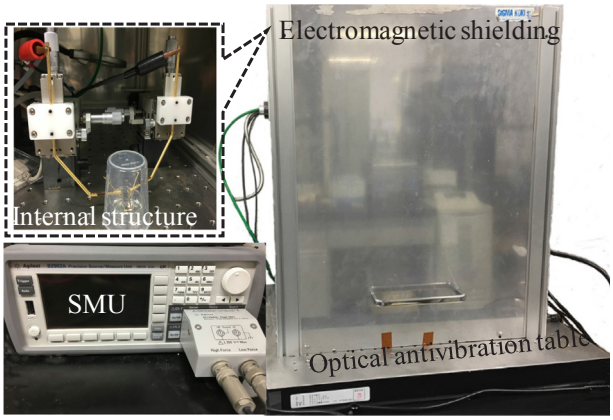

Fig. 2. Configuration of the high precision current-voltage measurement system.

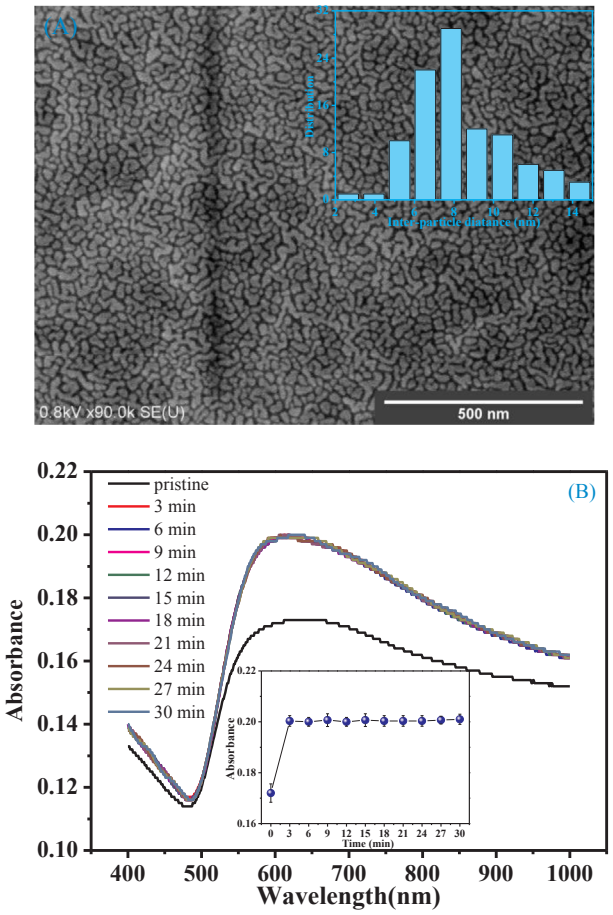

Fig. 3. (A) Morphological and (B) spectral characteristics of as-sputtered Au nano-island film in air and in ethanol (inset in (A): inter-particle distance distribution, inset in (B): absorbance value versus time).

3. Results and discussion

3.1. Optical characteristics of Au nano-islands film in ethanol

The morphology and spectral characteristics of the as-sputtered Au nano-islands are shown in Fig. 3. The Au nano-islands had an irregular shape with a tightly packed pattern and complex cross-linked structure. According to our previous work, this structure provides many effective current pathways. The area of coverage of the Au nano-islands was as high as 68.73%, based on calculations with the software Image J. The absorption spectra of the sputtered Au nano-islands film before and after immersion in ethanol [Fig. 3(B)] showed characteristics consistent with their structural features. The spectrum of the as-sputtered Au nano-islands film had a wide LSPR peak, which we mainly attribute to the morphology and inter-island distance. When immersed in an ethanol solution, the absorbance of islands film increased, which we attribute to the increased refractive index (RI) around the nano-islands from air (n = 1.00) to ethanol (n = 1.33). Furthermore, the bandwidth of the absorbance spectra narrowed compared with that in air. We attribute this change to the balance of RI on either sides of the nano-islands. As the surrounding medium was changed from air to ethanol, the RI difference beside the Au nano-islands decreased (glass substrate: n = 1.50). Moreover, there was almost no variation of the absorbance magnitude versus immersion time. Therefore, we conclude that the Au nano-islands film in ethanol remained stable (at least during the measuring period). These results also suggested a short response time of the Au nano-islands to the surrounding RI change (less than 3 min).

3.2. Optical characteristics of the Au nano-islands film in thiolate ethanol solution

The thiolate molecules bound to the surface of the Au nanoparticles through Au-S bonding, which changed the optical characteristics of Au nanoparticles [16–19]. The main explanation to this phenomenon is a reduction of the electron density in the NPs, and an increase of damping owing to charge localization at the NP surface. In a recent report, Lica et al. proposed that the absorbance changes because of the decreased density of Au 5*d* electrons caused by charge transfer from the Au atoms

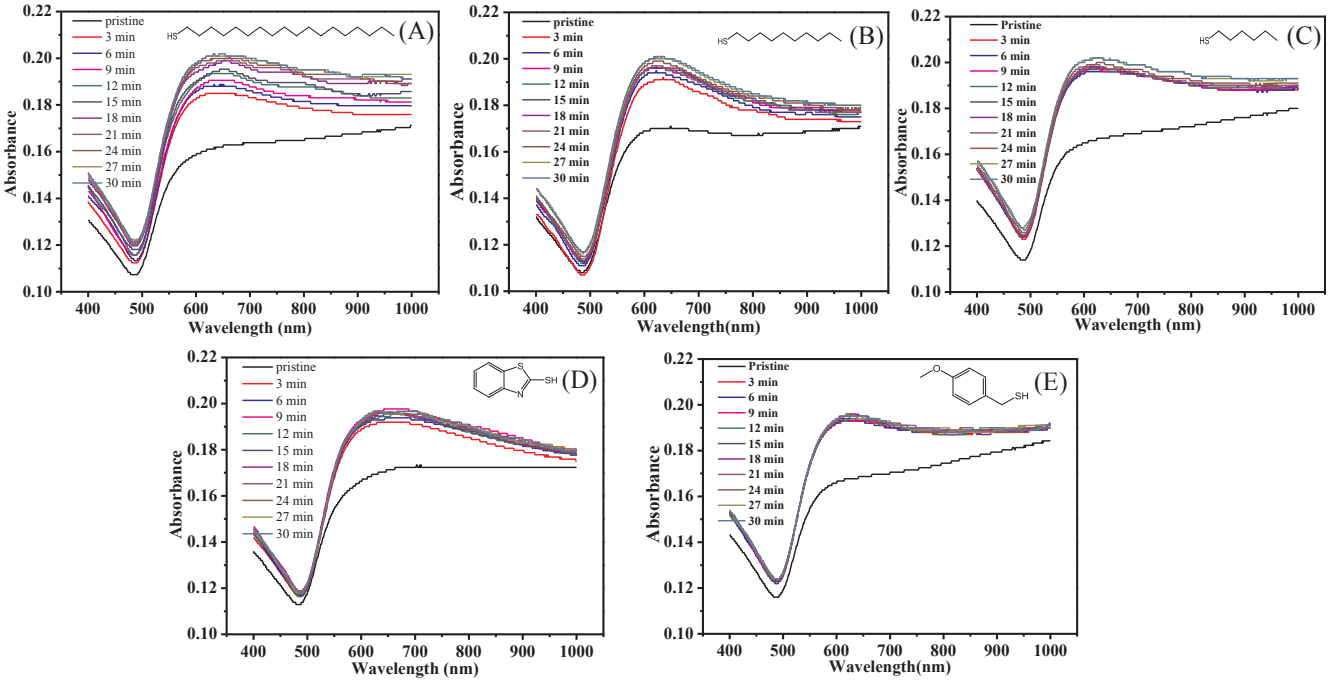

Fig. 4. Time-dependent spectral characteristics of Au nano-island film immersed in (A) 1-octadecanethiol, (B) 1, 10-decanethiol, (C) 1-hexanethiol, (D) 2-mercaptobenzothiazole, (E) 4-methoxy-α-toluenethiol ethanol solution (thiolate concentration: 0.5 μM).

to the S atoms of the thiolates [21]. Charge localization at the Au-S bond blocks electrons involved in bonding at the NP surface [20,22]. The localization of charge interacts electrostatically with NP conduction electrons, inducing extra damping in electrons oscillation, known as chemical interface damping, which increases the spectral bandwidth [23–24]. Herein, five kinds of thiolates were selected to analyze the time-dependent binding process of the thiolate molecules to the Au nano-islands, namely, 2-mercaptobenzothiazole, 1,10-decanethiol, 1-octadecanethiol, 1-hexanethiol and 4-methoxy-α-toluenethiol. Spectra of the Au nano-islands film in various thiolate ethanol solutions were recorded over 30 min. As illustrated in Fig. 4, thiolate binding to the surface of the nano-islands increased the optical absorbance. This phenomenon differs from some reports in which thiolate binding resulted in weakening and even the disappearance of the LSPR [25,26]. We attributed this difference to size effects of the nanoparticles used in the current study.

Some studies have demonstrated that electromagnetic field decay from the Au nanoparticle surface is size-dependent with a range less than 20 nm, and the RI change greatly influences the corresponding spectral characteristics [27–29]. When immersed in thiolate solution, the amount of thiolate molecules within the range of the electromagnetic field increased, particularly those bonded to the surface of the Au nano-islands, and increased RI. Hence, the increase induced by the thiolate molecules likely played an important role. The maximum absorbance of the thiolate ethanol solution is defined as A, and the maximum absorbance value in air is defined as A_0. The parameters $(A-A_0)/A_0$ for different types of thiolate molecule are summarized in Fig. 5. Notably, the value of $(A-A_0)/A_0$ depends on the thiolate structure. For example, 1-octadecanethiol with a long alkane chain induced a relatively large $(A-A_0)/A_0$ increase versus time. Whereas thiolates with the short alkane chains and ring structures induced a relatively small increase. The electron transfer process occurs during in the binding process between thiolate molecules; hence, the binding to the Au nano-islands could not be comprehensively studied by optical methods.

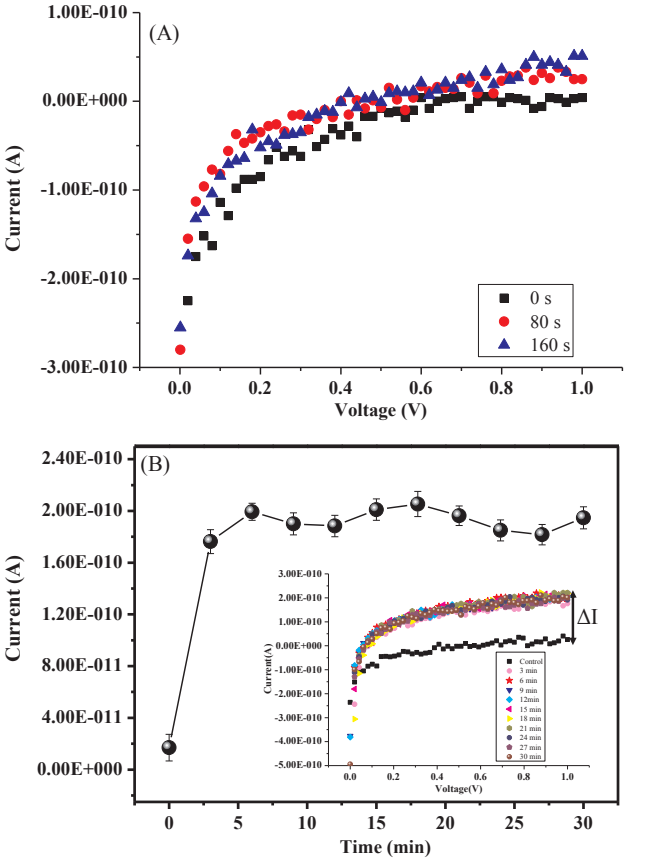

Fig. 6. (A) Current characteristics of IME@AuNI versus Au sputtering time, (B) Time-dependent voltage-current characteristics of IME@AuNI immersed in ethanol (insert: current-voltage curve scanned at 3-min intervals).

3.3. Voltage-current characteristics of IME@AuNI in thiolate ethanol solution

Voltage-current characteristics of IME@AuNI versus sputtering time are compared, as shown in Fig. 6(A). The current of the bare IME was close to 0 pA but increased to several tens of picoampere after sputtering of the nano-islands. For Au sputtering times longer than 240 s,

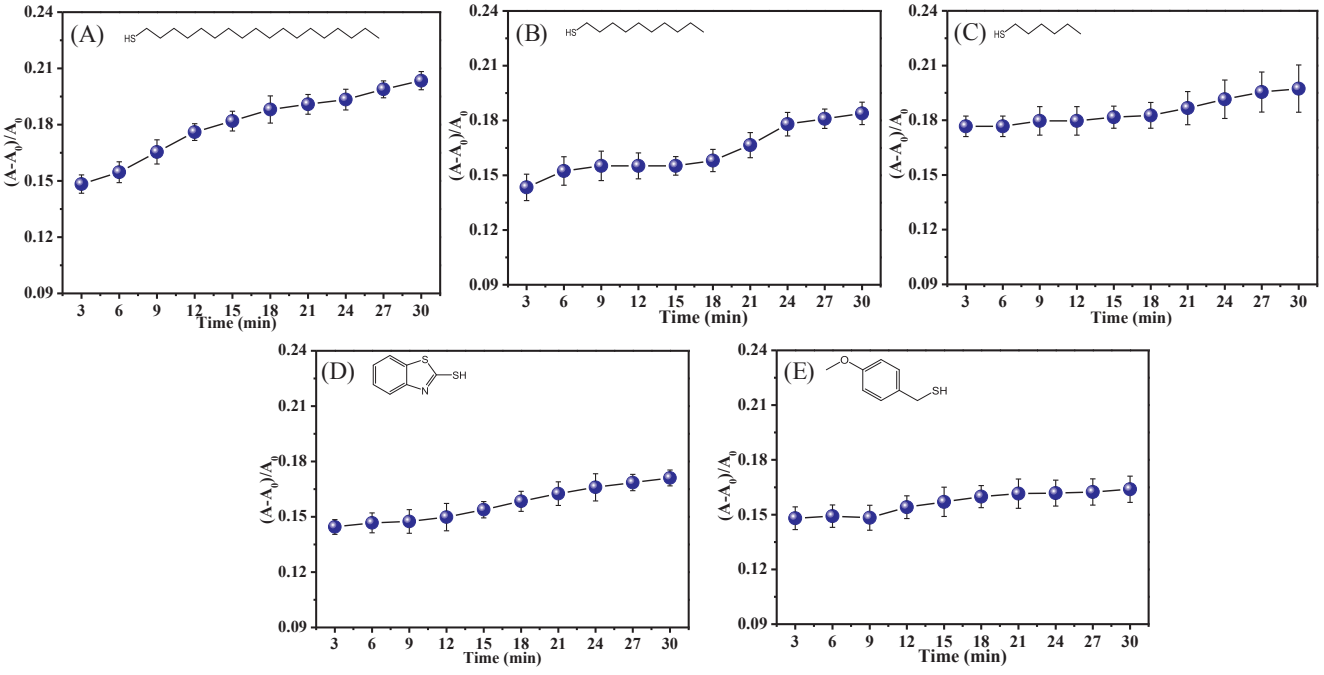

Fig. 5. $(A - A_0)/A_0$ versus thiolate type over extended immersion times.

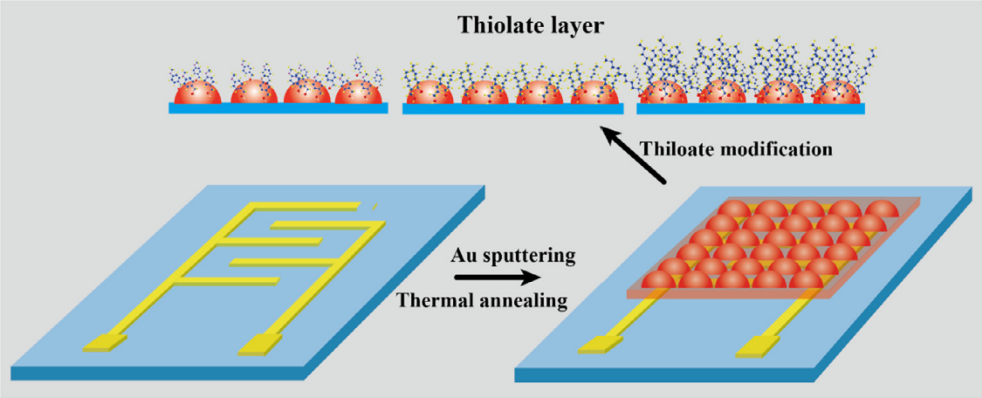

Scheme 1. IME@AuNI with thiolate molecule capping layers.

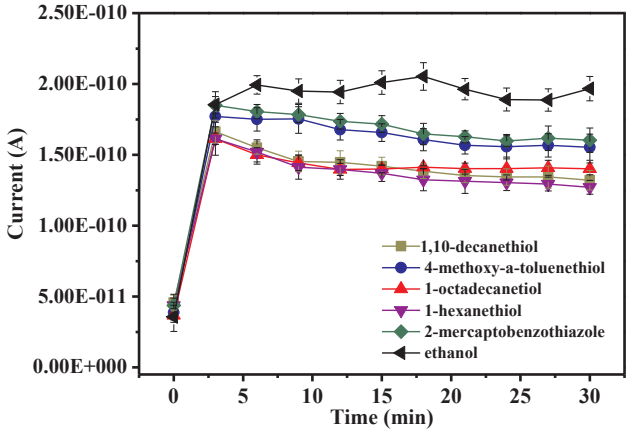

Fig. 7. Current-voltage curve of IME@AuNI versus immersion time in thiolate ethanol solution (thiolate concentration: 0.5 μm).

the current baseline became excessively high. Hence, the optimal sputtering time of 160 s was used. The structure of IME@AuNI is illustrated in Scheme 1. As the medium was changed from air to ethanol, the current increased to nearly 200 pA [Fig. 6(B)], which we explain by the medium variation inducing a conductance increase [30,31]. Furthermore, according to the result shown in Fig. 3(A), the average inter-islands distance was approximately 8.3 nm (counted from 100 samples using the software Nano measure). Leifer and coworkers [32] observed the Fowler–Nordheim tunneling effect in nano-electrodes with sub-5 nm nanogaps; however, for larger nanogaps (> 5 nm), Fowler–-Nordheim tunneling was not found. Consequently, the tunneling current among the Au nano-islands in this present work is mainly classified as direct tunneling current [32–34]. Moreover, in the current-voltage curve, when the applied voltage was small, the current had a negative value, which might be caused by capacitive and impedance effects from the Au nanoparticle film and IME substrate [35]. The randomness of the sputtered Au nano-islands might lead to more AuNPs deposited on one electrode than on others. This effect might produce some asymmetry of the current-voltage curves but is unlikely to have such a strong effect [32]. Stable current curves and optical characteristics versus time were observed when IME@AuNI was immersed in ethanol. When immersed in thiolate ethanol solution, thiolate molecules formed a structure-dependent capping layer on nano-islands with various distributions and densities [36,37]. The time-dependent current characteristics of IME@AuNI immersed in five kinds of thiolate ethanol solution are summarized in Fig. 7. The current of IME@AuNI showed a tendency to decrease over time, which we mainly attribute to electron transfer induced by thiolate binding, which decreased the tunneling current among the nano-islands. Furthermore, we inferred that the thiolate structure also affected the time-dependent current characteristics [38]. Here, 1-octadecanethiol and 1-decanethiol with long chain structure induced a current decrease that was more obvious than that of 2-mercaptobenzothiazole and 4-methoxy-α-toluenethiol. Moreover, the bridging effect of the thiolate molecules among the Au nano-islands was non-negligible, particularly for 1-octadecanethiol. The long chain structure of 1-octadecanethiol might make it more prone to bridging effects among nano-islands. In summary, we attribute the current decrease to two aspects. First, electron transfer from Au nano-islands to thiolate molecules anchored on the surface of Au nano-islands. The thiolate molecules might be prone to forming a structure dependent monolayer with different densities [39–42]. Second, the bridging effect of thiolate molecules among Au nano-islands is non-negligible.

4. Conclusion

We studied the optical and electrical characteristics of IME@AuNI immersed in five kinds of thiolate solution. Our results demonstrate that thiolate molecules bind to the surface of Au nano-islands and enhance absorbance in LSPR characteristics. The current of IME@AuNI tended to decrease when immersed in thiolate ethanol solution. We attribute this behavior to the electron transfer from the Au nano-islands to the thiolate molecules and bridging effects of the thiolate molecules among the Au nano-islands. We note that the electron transfer process was directly observed by this direct electrical measuring approach. We believe that this approach could also provide a new way to investigate and improve the performance of nano-devices, which depend on electron transfer.

Acknowledgements

This study was supported by National Nature Science Foundation of China Nos. 61801400, and 61703348, Central Universities under Grant numbers XDJK2018C021, and JSPS KAKENHI Grant Number JP18F18392.

References

[1] F. Prins, A. Barreiro, J.W. Ruitenberg, J.S. Seldenthuis, N. Aliaga-Alcalde, L.M.K. Vandersypen, H.S.J. van der Zant, Room-temperature gating of molecular junctions using few-layer graphene nanogap electrodes, Nano Lett. 11 (2011) 4607–4611.
[2] A. Schenk, G. Heiser, Modeling and simulation of tunneling through ultra-thin gate dielectrics, J. Appl. Phys. 81 (1997) 7900–7908.
[3] T.S. Metzger, R. Tel-Vered, I. Willner, Controlled vectorial electron transfer and photoelectrochemical applications of layered relay/photosensitizer-imprinted au nanoparticle architectures on electrodes, Small 12 (2016) 1605–1614.
[4] J.J. Fan, Z.Z. Li, W.Y. Zhou, Y.C. Miao, Y.J. Zhang, J.H. Hu, G.S. Shao, Dye-sensitized solar cells based on TiO_2 nanoparticles/nanobelts double-layered film with improved photovoltaic performance, Appl. Surf. Sci. 319 (2014) 75–82.
[5] H. Ran, J. Fan, X. Zhang, J. Mao, G. Shao, Enhanced performances of dye-sensitized solar cells based on Au-TiO_2 and Ag-TiO_2 plasmonic hybrid nanocomposites, Appl.

Surf. Sci. 430 (2018) 415–423.
[6] V. Subramanian, E.E. Wolf, P.V. Kamat, Catalysis with TiO_2/gold nanocomposites. Effect of metal particle size on the Fermi level equilibration, J. Am. Chem. Soc. 126 (2004) 4943–4950.
[7] Y.W. Su, J.Y. Yeh, H.C. Tsai, R.C. Tsiang, Enhanced performance of P3HT/TiO_2 bilayer heterojunction photovoltaic device having gold nanoparticles in the donor layer, J. Nanosci Nanotechnol. 11 (2011) 10027–10035.
[8] P.S. Jensen, Q. Chi, F.B. Grumsen, J.M. Abad, A. Horsewell, D.J. Schiffrin, J. Ulstrup, Gold nanoparticle assisted assembly of a heme protein for enhancement of long-range interfacial electron transfer, J. Phys. Chem. C 111 (2007) 6124–6132.
[9] G. Lei, P.F. Gao, T. Yang, J. Zhou, H.Z. Zhang, S.S. Shan, M.X. Gao, C.Z. Huang, Photoinduced electron transfer process visualized on single silver nanoparticles, ACS Nano 11 (2017) 2085–2093.
[10] A.E. Schlather, A. Manjavacas, A. Lauchner, V.S. Marangoni, C.J. DeSantis, P. Nordlander, N.J. Halas, Hot hole photoelectrochemistry on Au@SiO_2@Au nanoparticles, J. Phys. Chem. Lett. 8 (2017) 2060–2067.
[11] M. Zhao, H. Xu, S. Ouyang, D. Li, X. Meng, J. Ye, Effect of band structure on the hot-electron transfer over Au photosensitized brookite TiO_2, Phys. Chem. Chem. Phys. 18 (2016) 3409–3412.
[12] S.L. Young, J.E. Kellon, J.E. Hutchison, Small gold nanoparticles interfaced to electrodes through molecular linkers: a platform to enhance electron transfer and increase electrochemically active surface area, J. Am. Chem. Soc. 138 (2016) 13975–13984.
[13] B. Chen, C. Liu, L. Ge, K. Hayashi, Electrical conduction and gas sensing characteristics of P3HT/Au nano-islands composite, Sens. Actuators, B 241 (2017) 1099–1105.
[14] B. Chen, M. Mokume, C. Liu, K. Hayashi, Irradiation wavelength-dependent photocurrent sensing characteristics of AuNPs/P3HT composites on volatile vapor, IEEE Sens. J. 16 (3) (2016) 596–602.
[15] B. Chen, M. Mokume, C. Liu, K. Hayashi, Structure and localized surface plasmon tuning of sputtered Au nano-islands through thermal annealing, Vacuum 110 (2014) 94–101.
[16] B. Chen, C. Liu, L. Ge, K. Hayashi, Localized surface plasmon resonance gas sensor of Au nano-islands coated with molecularly imprinted polymer: influence of polymer thickness on sensitivity and selectivity, Sens. Actuators, B 231 (2016) 787–792.
[17] J.R. Reimersa, M.J. Fordb, A. Halderc, J. Ulstrupc, N.S. Hush, Gold surfaces and nanoparticles are protected by Au(0)-thiyl species and are destroyed when Au(I)-thiolates form, PNAS 113 (2016) 1424–1433.
[18] J.R. Reimers, M.J. Ford, S.M. Marcuccio, J. Ulstrup, N.S. Hush, Competition of van der Waals and chemical forces on gold-sulfur surfaces and nanoparticles, Nat. Rev. Chem. 1 (2017) 1–25.
[19] Q. Chi, M.J. Ford, A. Halder, N.S. Hush, J.R. Reimers, J. Ulstrup, Sulfur ligand mediated electrochemistry of gold surfaces and nanoparticles: what, how, and why, Curr. Opin. Electrochem. 1 (2017) 7–15.
[20] L. Chen, Y. Huang, L. Ge, T. Yang, B. Chen, C.Z. Huang, A portable multi-channel sensing device using Au nano-urchins as probes for melamine detection in milk, J. Mater. Chem. C 5 (2017) 7806–7812.
[21] M. Yu, N. Bovet, C.J. Satterley, S. Bengió, K.R.J. Lovelock, P.K. Milligan, R.G. Jones, D.P. Woodruff, V. Dhanak, True nature of an archetypal self-assembly system: mobile Au-thiolate species on Au (1 1 1), Phys. Rev. Lett. 97 (2006) 166102.
[22] M.A. Garcia, J. Venta, P. Crespo, J. Lopis, S. Penadés, A. Fernández, A. Hernando, Surface plasmon resonance of capped Au nanoparticles, Phys. Rev. B 72 (2005) 241403-1–4.
[23] P. Zhang, T.K. Sham, Tuning the electronic behavior of Au nanoparticles with capping molecules, Appl. Phys. Lett. 81 (2002) 736–738.
[24] P. Zhang, T.K. Sham, X-ray studies of the structure and electronic behavior of alkanethiolate-capped gold nanoparticles: the interplay of size and surface effects, Phys. Rev. Lett. 90 (2003) 245502-1–4.
[25] J. Zheng, C. Zhang, R.M. Dickson, Highly fluorescent, water-soluble, size-tunable gold quantum dots, Phys. Rev. Lett. 93 (2004) 077402-1–4.
[26] G.C. Lica, B.S. Zelakiewicz, M. Constantinescu, Y. Tong, Charge dependence of surface plasma resonance on 2 nm octanethiol-protected Au nanoparticles: evidence of a free-electron system, J. Phys. Chem. B 108 (2004) 19896–19900.
[27] M.D. Malinsky, K.L. Kelly, G.C. Schatz, R.P. Van Duyne, Chain length dependence and sensing capabilities of the localized surface plasmon resonance of silver nanoparticles chemically modified with alkanethiol self-assembled monolayers, J. Am. Chem. Soc. 123 (2001) 1471–1482.
[28] A.J. Haes, S. Zou, G.C. Schatz, R.P. Van Duyne, A nanoscale optical biosensor: the long range distance dependence of the localized surface plasmon resonance of noble metal nanoparticles, J. Phys. Chem. B 108 (1) (2004) 109–116.
[29] A.J. Haes, S. Zou, G.C. Schatz, R.P. Van Duyne, Nanoscale optical biosensor: short range distance dependence of the localized surface plasmon resonance of noble metal nanoparticles, J. Phys. Chem. B 108 (22) (2004) 6961–6968.
[30] P.A. Reissner, J. Tisserant, A. Sánchez-Ferrer, R. Mezzenga, A. Stemmer, Solvent-mediated conductance increase of dodecanethiol-stabilized gold nanoparticle monolayers, Beilstein J. Nanotechnol. 7 (2016) 2057–2064.
[31] N. Yang, W.K. Henson, J.R. Hauser, J.J. Wortman, Modeling study of ultrathin gate oxides using direct tunneling current and capacitance-voltage measurements in MOS devices, IEEE Trans. Electron Dev. 46 (7) (1999) 1464–1471.
[32] H. Li, I.H. Wani, A. Hayat, S.H.M. Jafri, K. Leifer, Fabrication of reproducible sub-5 nm nanogaps by a focused ion beam and observation of Fowler-Nordheim tunneling, Appl. Phys. Lett. 107 (2015) 103108.
[33] L.F. Register, E. Rosenbaum, K. Yang, Analytic model for direct tunneling current in polycrystalline silicon-gate metal-oxide-semiconductor devices, Appl. Phys. Lett. 74 (3) (1999) 457–459.
[34] J.G. Simmons, Generalized formula for the electric tunnel effect between similar electrodes separated by a thin insulating film, J. Phys. Lett. 34 (6) (1963) 1793–1803.
[35] C.R. Bradbury, J. Zhao, D.J. Fermín, Distance-independent charge-transfer resistance at gold electrodes modified by thiol monolayers and metal nanoparticles, J. Phys. Chem. C 112 (2008) 10153–10160.
[36] J. Nishigaki, R. Tsunoyama, H. Tsunoyama, N. Ichikuni, S. Yamazoe, Y. Negishi, M. Ito, T. Matsuo, K. Tamao, T. Tsukuda, A new binding motif of sterically demanding thiolates on a gold cluster, J. Am. Chem. Soc. 134 (2012) 14295–14297.
[37] P.D. Jadzinsky, G. Calero, C.J. Ackerson, D.A. Bushnell, R.D. Kornberg, Structure of a thiol monolayer-protected gold nanoparticle at 1.1 Å resolution, Science 318 (2007) 430–433.
[38] Y. Wang, Q. Chi, J. Zhang, N.S. Hush, J.R. Reimers, J. Ulstrup, Chain-branching control of the atomic structure of alkanethiol-based goldsulfur interfaces, J. Am. Chem. Soc. 133 (2011) 14856–14859.
[39] B. Chen, C. Liu, M. Ota, K. Hayashi, Terpene detection based on localized surface plasma resonance of thiolate-modified Au nanoparticles, IEEE Sens. J. 13 (4) (2013) 1307–1314.
[40] M.D. Musick, C.D. Keating, Metal films prepared by stepwise assembly. 2. Construction and characterization of colloidal Au and Ag multilayers, Chem. Mater. 12 (10) (2000) 2869–2881.
[41] T. Hayashi, Y. Morikawa, H. Nozoye, Adsorption state of dimethyl disulfide on Au (1 1 1): evidence for adsorption as thiolate at the bridge site, J. Chem. Phys. 14 (17) (2001) 7615–7621.
[42] M. Stobiecka, K. Coopersmith, M. Hepel, Resonance elastic light scattering (RELS) spectroscopy of fast non-Langmuirian ligand-exchange in glutathione-induced gold nanoparticle assembly, J. Colloid Interf. Sci. 350 (2010) 168–177.